# Measurement of the viscosity coefficient $\eta_3$ in free-standing smectic films

F. Schneider
*Physikalische Chemie, Universität Siegen, 57068 Siegen, Germany*
(Received 27 April 2006; published 23 August 2006)

Thinner parts (the so-called holes) and thicker parts (islands) move in free-standing smectic films due to gravity if the film is inclined. The velocity of the movement depends on the viscosity coefficient $\eta_3$ of the film. Therefore, this measurement is a direct method to determine $\eta_3$ in smectic phases. This paper contains the corresponding hydrodynamic calculations for the flow patterns in and around a circular hole in a circular two-dimensional film under various conditions. The viscous force on the hole is calculated. Experiments are performed with the liquid crystal *n*-octyl-cyano-biphenyl (8CB) in the smectic phase. The influence of the disclination which surrounds the hole and the influence of the gas which surrounds the film on the movement is studied. It is shown that the influence of these effects on the determination of $\eta_3$ can be neglected if the film is thick and the difference in the thicknesses between film and hole is small. The temperature dependence of $\eta_3$ is determined for 8CB.

DOI: 10.1103/PhysRevE.74.021709 PACS number(s): 61.30.−v, 68.15.+e, 66.20.+d, 47.15.−x

## I. INTRODUCTION

The viscous behavior of nematic liquid crystals has been studied in numerous papers [1–3]. The viscosity coefficients—especially the rotational viscosity coefficient $\gamma_1$—are used to calculate the switching times of liquid crystal displays. The number of papers which are concerned with the measurement in smectic phases is very small. For some smectic phases—i.e., in $S_C$ phases [4]—the viscous behavior is very complicated. For all smectic phases it is difficult to align the director and to avoid the generation of disclinations during the experiment. Use of free-standing smectic films avoids this problem.

Free-standing films have the unique property of perfect alignment of the director and constant thickness over large areas. It is very simple to draw films with thicknesses between two and several thousand molecular lengths with areas of some $cm^2$. Furthermore, it is possible to generate circular areas with a smaller or larger thickness in a film. Areas with a smaller thickness (holes) can be generated by a heating technique developed by Géminard *et al.* [5]. If the film is inclined, the holes and islands begin to move [6] and the viscosity coefficient $\eta_3$ can be determined from the gravitational force on the hole or island and the viscous drag.

## II. EXPERIMENT

### A. Experimental methods

Films were drawn with a wiper across a 14-mm aperture in a film holder made from aluminum (see Fig. 1). The wiper is moved by means of a motor-driven micrometer screw. For thick films up to 30 $\mu$m the wiper velocity is 0.01 mm/s. Thin films are drawn with velocities up to 8 mm/s. The measurements are performed under hydrogen or nitrogen (both 99.999%).

The holes are generated with a heating element (Géminard *et al.* [5]) which consists of a 30-$\mu$m stainless steal wire. The upper part of the wire is covered with a 30-$\mu$m silver film in order to release the heat at the sharp kink which is mounted some 10 $\mu$m above the film. The pulse generator is a regulated power supply and a 1-F capacity which is loaded up to 1–15 V and is connected for 0.1–1 ms with the heating element.

The film and film holder are surrounded by a thermostatted housing with a temperature stability of ±0.01 K. Two inclined glass windows allow the observation of the film from above and below. Additional glass windows are used to maintain a constant temperature at the film and to avoid flow of the gas in the housing. Light traps and apertures avoid

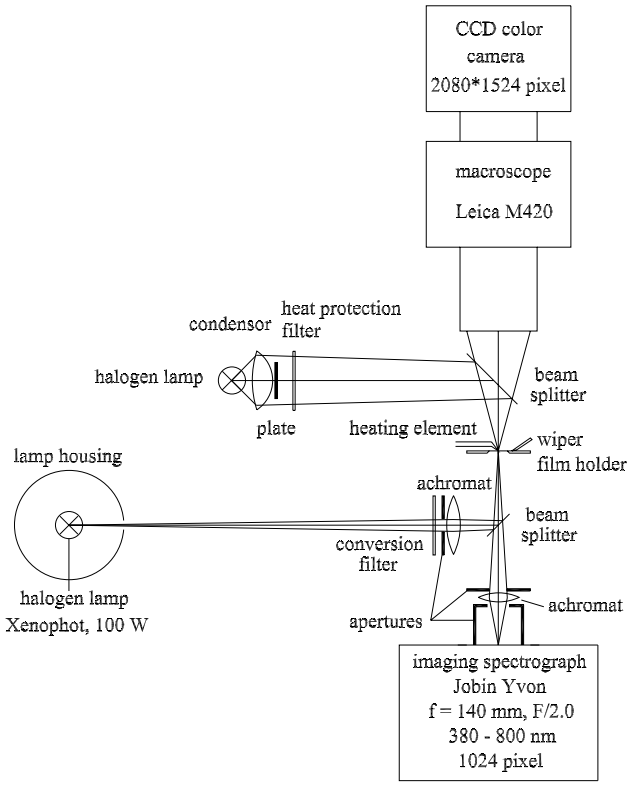


FIG. 1. Schematic diagram of the setup. The thermostatted housing for the film, windows in the housing, light traps, and motor-driven micrometer screw for the wiper movement are not shown.

 

stray light in the upper and lower optical paths.

Visual observation of the film during drawing is performed with a macroscope (microscope with a small magnification and a large working distance, Leica, M420). Coaxial illumination with a usual microscope illuminator is accomplished by means of a beam splitter made from a 0.15-mm glass plate. As the image contrast from the disclination at the border of the hole is small a simple dark-field illumination is used which consists of a plate at the condenser of the macroscope illumination and an aperture in the macroscope. The movement of the holes is recorded by means of a camera (QImaging, MicroPublisher, cooled version) with up to two frames per second.

The thickness of the films is measured by means of interference spectra which are measured in reflection. The light source is a halogen lamp (Osram, Xenophot, 100 W). The filament is imaged on the film by means of an achromat. An aperture of 4 mm gives a maximum deviation from normal incidence of 1°. The conversion filter (Linos, TL60) reduces the light intensity at the wavelength of the maximum signal of the imaging spectrograph and transmits the light at short and long wavelengths.

The spectra are recorded with an imaging spectrograph (Jobin Yvon, $f=140$ mm, 375–800 nm, 1024 pixels). After calibration with 30 spectral lines between 378 nm (Tl) and 795 nm (Rb) the precision of the wavelength determination of the interference spectra is better than 0.1 nm. A 16-bit intensity resolution and averaging of the recordings (20 – 100 times) resulted in spectra with high signal-to-noise ratios.

The whole setup could be rotated around a horizontal axis in order to incline the film. Usual inclination angles are 3°–7°.

The measurements were performed with the liquid crystal *n*-octyl-cyano-biphenyl (8CB), which exhibits an $S_A$ phase between 21.0 and 33.0 °C. The purity of 8CB (Synthon GmbH, Wolfen, Germany) was 99%.

Very thick films show a bending due to gravity. In the horizontal position the bending $z$ is (see Appendix B; $R_f$: film radius)

$$z = \frac{A}{4}(r^2 - R_f^2) \quad \text{with} \quad A = \frac{\rho_d g d}{2\sigma}. \tag{1}$$

It amounts to −50 $\mu$m at the film center with respect to the film holder, and the deviation from the horizontal plane amounts to 0.8° at the film holder for a film with a thickness $d=25$ $\mu$m, a diameter of 14 mm, a density $\rho_d=1$ g/cm$^3$ (8CB), and a surface tension $\sigma=30$ mN/m (8CB [7]). Due to this bending, the vertical position of the heater has to be adjusted corresponding to the thickness of the film. The bending does not change the inclination of the film in the film center and has not to be taken into account in the evaluation of the gravitational force on the hole.

### B. Evaluation of measurements

The evaluation of the interference spectra is described in an earlier paper [8]. A measurement before the flow experiment gives the thickness $d_f$ of the outer part of the film. A second measurement after the hole has spread over the whole film gives the thickness $d_h$ of the hole. The resolution of the thickness measurement is some 0.1 nm so that the depth of holes with a depth of 30 nm can be determined with sufficient resolution.

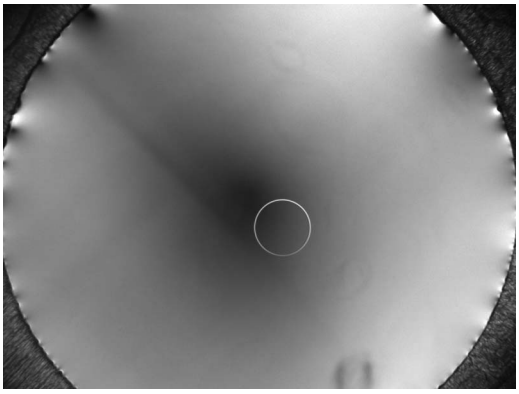

FIG. 2. Film with hole. The film holder (diameter 14 mm) is visible in the corners of the image. The variation of the intensity of the light reflected from the film is due to imperfections of the dark-field illumination and dust particles on the windows.

The holes were generated with the film in the horizontal position about 1 mm "below" the film center. Then the film was inclined and the movement was observed. Only those hole positions are used for the following evaluation for which the distance to the film center is smaller than 0.5 mm in order to fulfill the condition of concentricity which is assumed in the hydrodynamical calculations. Figure 2 shows a hole with a thickness difference of 1 $\mu$m which gives a high contrast. For usual measurements the contrast is so low that it would not be visible with the contrast and the resolution of the printed image.

The determination of the hole positions was performed with a program in a half automatic way. Finally a linear regression for usually ten positions gave the velocity of the hole.

The gravitational force on the hole is

$$F_g = \pi R_h^2 \rho_d g \Delta d \sin\beta, \tag{2}$$

where $R_h$ is the hole radius, $\rho_d$ the density of the liquid crystal, $\Delta d = d_f - d_h$ the depth of the hole, and $\beta$ the film inclination. Together with the hydrodynamical force [see Eq. (A14)] we find

$$R_h^2 \rho_d g \Delta d \sin\beta = \frac{-4\eta d_f V}{\ln\rho_h + \dfrac{1 + 2W - 4W\rho_h^2 - (1-2W)\rho_h^4}{2(1 + W + (1-W)\rho_h^4)}}, \tag{3}$$

which is the final equation for the evaluation of the viscosity. Some of the quantities are explained in Appendix A. In Eq. (3) and the following text the viscosity coefficient $\eta_3$ is designated with the abbreviation $\eta$. $\eta_3$ describes the viscosity for a flow with a director alignment perpendicular to the flow velocity and to the velocity gradient [9].

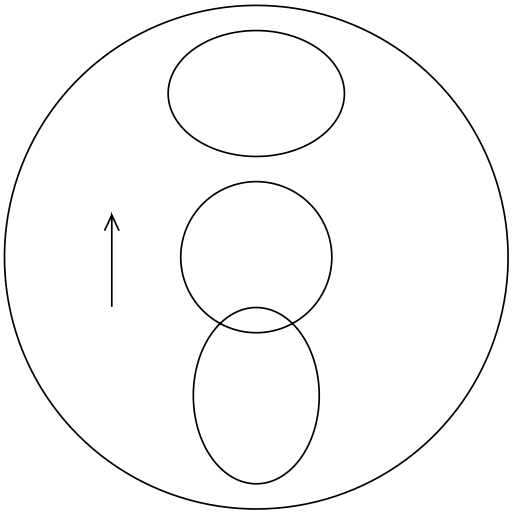

FIG. 3. Schematic drawing of the deformations of a moving hole at different positions in the film.

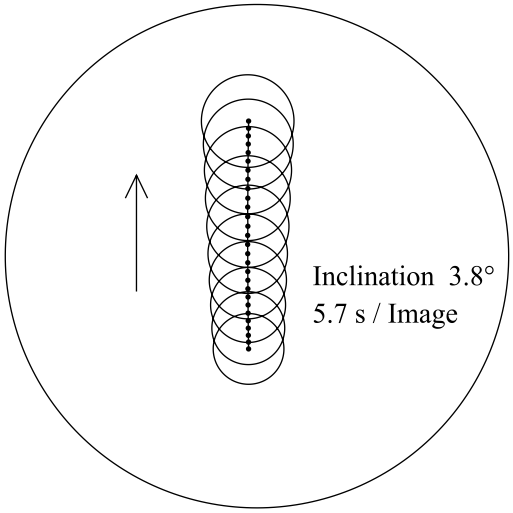


FIG. 4. Growing and movement of a hole in a film with a diameter of 14 mm. Each point (center of the hole) corresponds to a measurement. Not all perimeters are shown.

### C. Experimental results

The hole changes slightly its form during a motion over distances comparable with the film radius (see Fig. 3). If the hole starts near the film border, an elliptic distortion results with the long axis in the flow direction. This distortion is caused by the necessary flow of the liquid behind the hole. In the neighborhood of the center the hole is always circular due to the line tension of the disclination. If the hole approaches the film border, it is also elliptically distorted but with the long axis perpendicular to the flow direction. As only measurements with the hole near the film center were used for the further evaluation no problems resulted from the distortions of the holes near the film border.

During the movement of the hole hydrodynamic pressures act on it and can also lead to deviations from the circular form. Large holes are more easily deformed than small holes. This is first a consequence of the stronger hydrodynamic pressures on large holes due to their larger velocities. Second, a deviation of the bending of the disclination leads to a stronger deformation for a large hole than for a small hole. Under the usual experimental conditions—film inclination of some degrees and hole radii of 0.5–1 mm—this effect does not lead to noticeable deviations from the circular form of the holes.

Holes are growing if their radius is larger than the critical radius [5]. Due to the bending of the meniscus, the pressure in the film is smaller than the pressure in the surrounding gas. This leads to a force on the disclination which points to the outer side. Figure 4 shows the growing of a hole during the movement for a small inclination of the film—i.e., a slow movement. The increase of the hole radius leads to an accelerated movement and must be taken into account in the evaluation. The relative increase of the radius is small for the measurements used for the evaluation (distance to the film center smaller than 0.5 mm). Furthermore, in Eq. (3) the mean square of the hole radius $R_h$ is used as $R_h$ on the left side of Eq. (3), which contains the main dependence on $R_h$.

Figure 5 shows the apparent viscosity of 8CB at 22.0 °C under hydrogen and nitrogen as a function of the film thickness $d$. The apparent viscosity is calculated with Eq. (3) using the measured thickness ratio $W$. There is a structure in the scatter plot which is due to the sequence of measurements during one day. At the beginning a film with a certain thickness is drawn. Every hole reduces the film thickness somewhat and gives the film thickness for the next measurement.

There is a tendency to higher apparent viscosities with decreasing film thickness because the flow in the film leads to a flow and a dissipation of energy in the surrounding gas. The effect on the apparent viscosity of the film is reduced with increasing film thickness. The effect is more pronounced in nitrogen which exhibits a higher viscosity (17.5 $\mu$Pa s) than hydrogen (8.8 $\mu$Pa s, both at 20 °C).

The variation of the apparent viscosity at constant film thickness is due to the dissipation of energy in the disclination which surrounds the hole. This effect is discussed in the next paragraphs.

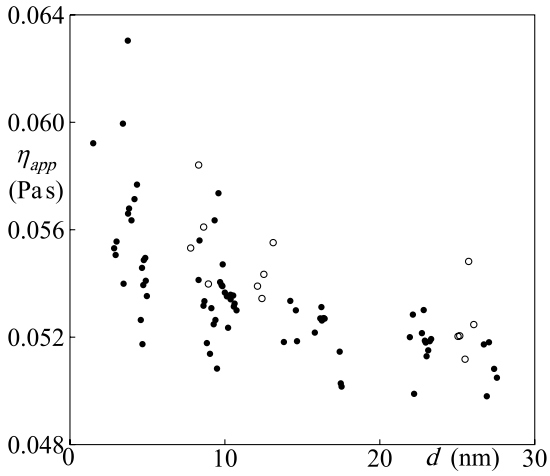


FIG. 5. Apparent viscosity $\eta_{app}$ of 8CB versus thickness $d$ of the film at 22.0 °C under hydrogen (•) and nitrogen (◦).

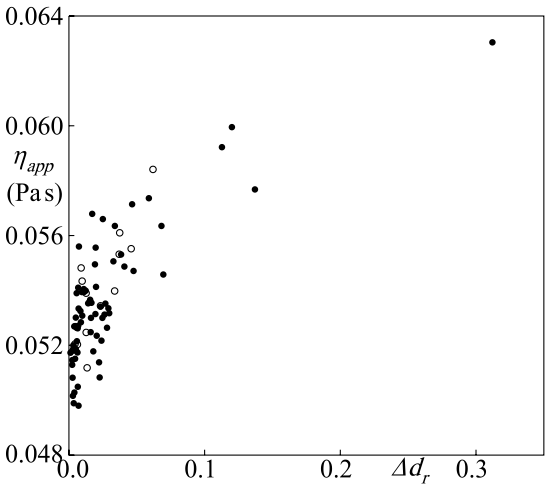


FIG. 6. Apparent viscosity $\eta_{app}$ of 8CB versus relative depth $\Delta d_r$ of the hole under hydrogen (•) and nitrogen (◦).

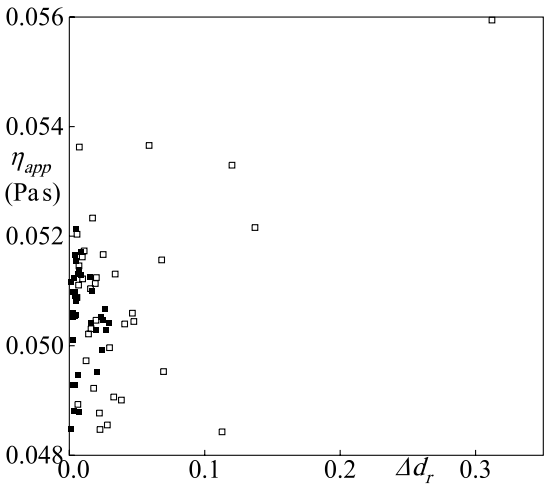


FIG. 7. Apparent viscosity $\eta_{app}$ of 8CB after correction for measurements under hydrogen. (■) Measurements in the range $d_f > 10\ \mu$ and $\Delta d_r < 0.04$, (□) measurements out of this range.

Figure 6 shows the same measurements as a function of the relative hole depth:

$$\Delta d_r = \Delta d/d_f = (d_f - d_h)/d_f. \tag{4}$$

In the derivation of Eq. (3) it was assumed that there is no energy dissipation in the disclination surrounding the hole. This leads to a flow in the hole (see Fig. 12 in Appendix A). The other extreme case is a strong dissipation because the line tension is high. The hole behaves like a solid plate (see Fig. 10, below). The drags for these cases ("fluid hole" and "solid hole") are different and their ratio is shown in Fig. 13, below.

The influence of the dissipation in the disclination on the apparent viscosity can be estimated as follows. The line tension of a disclination in thick films is proportional to $\Delta d$ [10]. Therefore, the energy dissipation in the disclination of a moving hole is also proportional to $\Delta d$ if all other quantities are held constant. The hydrodynamic energy dissipation in the film is proportional to $d_f$. Therefore, the apparent viscosity should depend on $\Delta d_r$ and the exact value should be found for $\Delta d_r \to 0$. Unfortunately, the dependence is not linear because very large $\Delta d_r$ values only lead to the case of the solid hole. The saturation of this dependence can be seen in Fig. 6. A simple ansatz for this dependence is

$$\eta_{app} = \eta\left[1 + \left(\frac{\eta_s}{\eta} - 1\right)\frac{\Delta d_r}{A + \Delta d_r}\right], \tag{5}$$

where $A$ is an unknown parameter and $\eta_s$ is the apparent viscosity for a solid hole if the determination of the viscosity is performed with the fluid hole equation (A16). $\eta_s/\eta$ corresponds to the inverse drag ratio of Eq. (A17). Equation (5) describes correctly the two limiting cases $\eta_{app} = \eta$ for $\Delta d_r \to 0$ and $\eta_{app} = \eta_s$ for $\Delta d_r \gg A$.

The second correction to be done is the influence of the gas. Here the ansatz

$$\eta_{app} = \eta + B/d_f \tag{6}$$

was used. This ansatz takes into account that the dissipation in the film is proportional to the film thickness $d_f$. $B$ is an unknown parameter.

The unknown parameters $A$ and $B$ in Eqs. (5) and (6) are determined by a least-squares fit from the experimental data. Figure 7 shows the success of this correction. The result is not perfect due to the simplicity of the equations and other effects which are not taken into account. One of those effects is the influence of the meniscus which is well visible in the upper left corner of Fig. 2. The width of the meniscus changes around the perimeter of the film (compare, e.g., the width of the menisci in the upper left and lower right corners of Fig. 2) and changes from one experiment to the other. It is to be assumed that there is no flow in the meniscus and that the effective film radius is smaller than the hole in the film holder.

As the correction for deep holes and thin films is not perfect it is better to avoid large corrections and to use only measurements on very thick films ($d_f > 10\ \mu$m) and on holes with small depths ($\Delta d_r < 0.04$) (see Fig. 7). In this case the simpler ansatz for the correction

$$\eta = \eta_{app} - C\Delta d/d_f - B/d_f \tag{7}$$

can be used.

Figure 8 shows the viscosity of 8CB as a function of temperature in the smectic phase and from 22 to 16 °C in the undercooled smectic phase. The thickness of the film was about 21 $\mu$m, and the hole depth varied from 0.014 to 0.04 $\mu$m. No correction due to the finite thickness and the nonzero hole depth was performed. The deviations from the solid line which is a fit with $\eta_0 \exp(E_a/RT)$ show the accessible precision of the method of measurement.

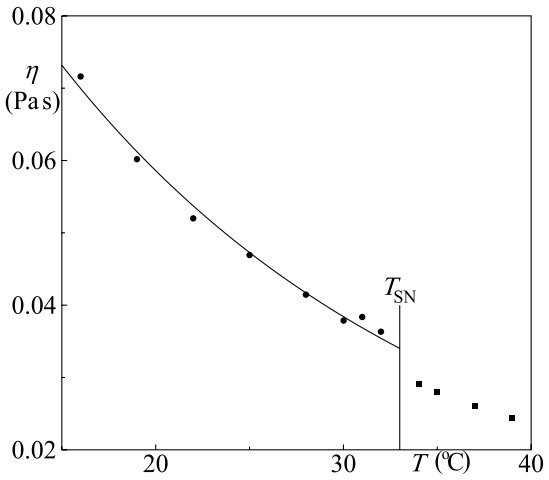


FIG. 8. Viscosity $\eta$ of 8CB versus temperature. (•) Measurements in the smectic phase (this work), (■) $\eta_3$ measurements in the nematic phase of 8CB from Kneppe *et al.* [11].

The values in the smectic phase are a continuation of the nematic values with a small offset. The nematic-smectic phase transition of 8CB is discussed to be continuous or to exhibit a very small transition enthalpy [12]. Therefore, it is to be assumed that the viscosity coefficient $\eta_3$ shows no sharp discontinuity at the transition. Small changes are expected due to small changes in the density.

Comparison with other measurements in smectic liquid crystals is difficult as there are only a few viscosity studies. Kim *et al.* [13] and Sohl *et al.* [14] have studied cyanobenzylidene octyloxyaniline (CBOOA) which is unstable and the melting point (84 °C) is rather high. They found out that the viscosity behaves nearly continuous at the nematic-smectic transition. The missing temperature dependence in the measurement of Sohl *et al.* is surely an experimental artifact. Bhattacharya and Letcher [15] and Krestov *et al.* [16] have studied two reentrant nematic mixtures of cyanobiphenyls and cyanoterphenyls with results similar to this paper. Thus, there is no direct comparison with other measurements on 8CB which is the standard smectic liquid crystal today.

## III. SUMMARY

Measurement of the velocity of moving holes in inclined free-standing smectic films allows the determination of the viscosity coefficient $\eta_3$. The hydrodynamics of the hole movement and errors of the determination is discussed. Measurements are performed with the room-temperature smectic liquid crystal 8CB. The temperature dependence of $\eta_3$ is determined and compared with the dependence in the nematic phase.

A disadvantage of the method is the limitation to the measurement of $\eta_3$.

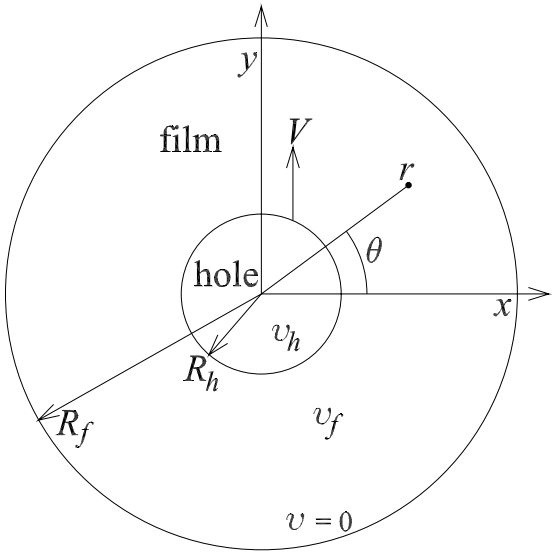


FIG. 9. Definition of quantities used in the hydrodynamical calculations. $\rho = r/R_f$ is the dimensionless radius.

## ACKNOWLEDGMENTS

We would like to thank Professor R. Jaquet and Professor G. Holzwarth, of The University of Siegen, for fruitful discussions on the film bending. Financial support by the Deutsche Forschungsgemeinschaft is gratefully appreciated.

## APPENDIX A: HYDRODYNAMICAL CALCULATIONS

In this appendix the flow pattern for the movement of a thinner part (a so-called hole) in a smectic film is calculated. The calculation is performed under the following assumptions.

(i) Two-dimensional laminar flow of an incompressible fluid.

(ii) Circular film and hole.

(iii) Concentric position of the hole.

(iv) No-slip condition at the outer boundary of the film.

(v) No energy dissipation in the disclination which surrounds the hole.

(vi) No influence of the gas above and below the film.

Under these conditions introduction of the stream function $\psi$ simplifies the calculation. The velocity components $v_x$ and $v_y$ are related to the stream function by

$$\frac{\partial \psi}{\partial y} = v_x, \quad \frac{\partial \psi}{\partial x} = -v_y, \tag{A1}$$

and the stream function must satisfy the two-dimensional biharmonic equation [17]

$$\nabla^4 \psi = 0. \tag{A2}$$

The general solution of the biharmonic equation in polar coordinates for a movement in the tilt direction $y$ is [17] (see Fig. 9)

$$\psi = \cos\theta (Ar + Br^{-1} + Cr^3 + Dr \ln r). \tag{A3}$$

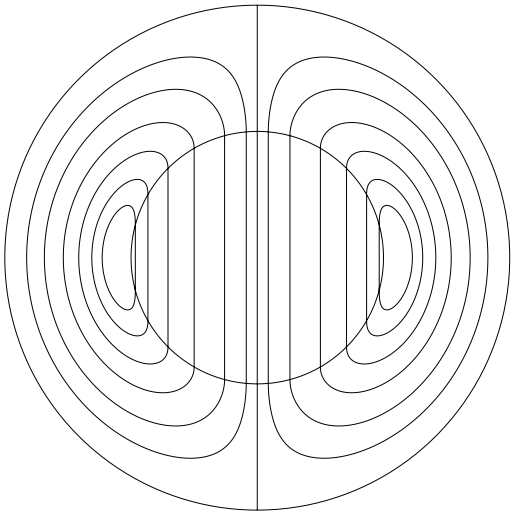

FIG. 10. Flow pattern around a moving solid hole.

The velocity components are obtained as

$$v_r = -\sin\theta(A + Br^{-2} + Cr^2 + D\ln r), \tag{A4}$$

$$v_\theta = -\cos\theta[A - Br^{-2} + 3Cr^2 + D(1 + \ln r)]. \tag{A5}$$

The constants $A$–$D$ have to be determined from the boundary conditions.

It is not known *a priori* whether there is a flow within the hole. A flow within the hole leads to changes in the length of the disclination line. One extreme case ("fluid hole") would be observed if the energy dissipation due to the changes in the disclination line can be neglected compared with the dissipation in the remaining part of the film. The other extreme case ("solid hole") would be observed if the energy dissipation in the disclination would be large and would prevent the flow within the hole. The solution for the solid hole has been reported by Slezkin [18] (see also [17]).

A general solution takes into account a fluid hole with a film thickness that is different from that in the outer part of the film. Because the different film thicknesses $d_f$ and $d_h$ cannot be used in a two-dimensional model, the viscosity in the hole is changed according to $\eta_h = \eta_f d_h / d_f$. Two different sets of constants $A_f$–$D_f$ and $A_h$–$D_h$ have now to be determined for the outer and inner flow. Correspondingly, eight boundary conditions have to be fulfilled.

Conditions at $R_f$:

$$\theta = 0^\circ : A_f - B_f R_f^{-2} + 3C_f R_f^2 + D_f(1 + \ln R_f) = 0,$$

$$\theta = 90^\circ : A_f + B_f R_f^{-2} + C_f R_f^2 + D_f \ln R_f = 0.$$

Conditions at $R_h$:

$$\theta = 90^\circ : -(A_f + B_f R_h^{-2} + C_f R_h^2 + D_f \ln R_h) = V,$$

$$\theta = 90^\circ : -(A_h + B_h R_h^{-2} + C_h R_h^2 + D_h \ln R_h) = V,$$

$$A_f - B_f R_h^{-2} + 3C_f R_h^2 + D_f(1 + \ln R_h) = A_h - B_h R_h^{-2} + 3C_h R_h^2 + D_h(1 + \ln R_h),$$

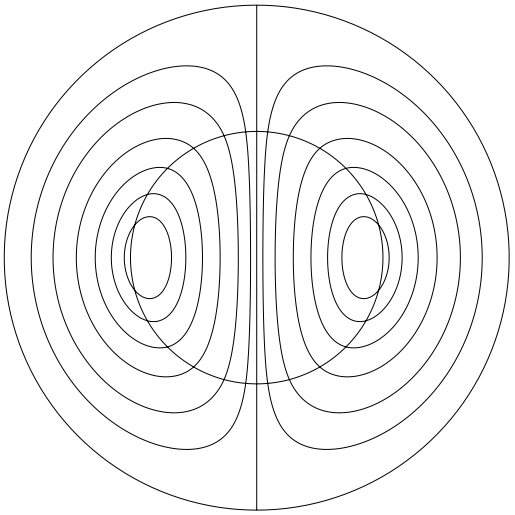

FIG. 11. Flow pattern for a moving fluid hole. The film thicknesses inside and outside are assumed to be equal.

$$\eta_f(B_f R_h^{-3} + C_f R_h) = \eta_h(B_h R_h^{-3} + C_h R_h).$$

Conditions at $r = 0$:

$$B_h = 0,$$

$$D_h = 0.$$

The last boundary condition at $R_h$ is due to the assumption of equal forces on both sides of the disclination.

The equations have been solved with Mathematica:

$$A_f = V\{1 + \rho_h^4(W - 1) + W - 2\rho_h^2 W + 2[-1 + \rho_h^4(W - 1) - W]\ln R_f\}/Z, \tag{A6}$$

$$B_f = -V\frac{R_f^2\rho_h^2[\rho_h^2(W - 1) - W]}{Z}, \tag{A7}$$

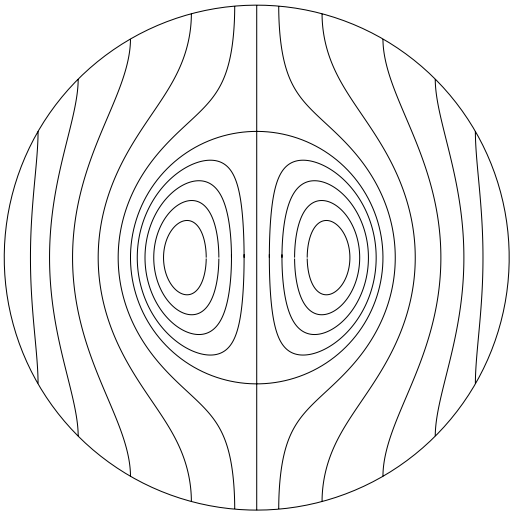

FIG. 12. Flow pattern for a fixed fluid hole in a film with a moving film holder.

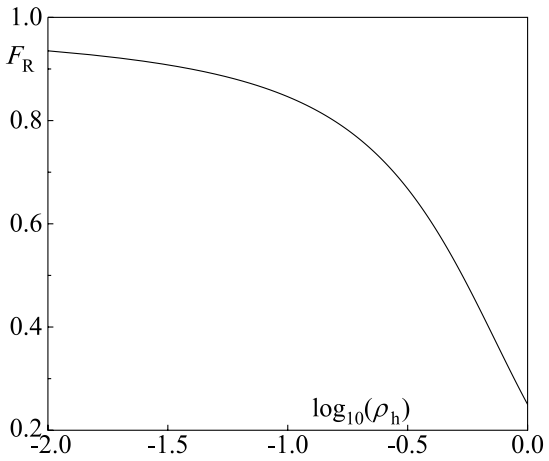


FIG. 13. Drag ratio for the fluid and solid hole as a function of the relative hole radius $\rho_h$.

$$C_f = V\frac{-1+(\rho_h^2-1)W}{R_f^2 Z}, \tag{A8}$$

$$D_f = 2V\frac{1-\rho_h^4(W-1)+W}{Z}, \tag{A9}$$

$$A_h = 2V\{(-1+\rho_h^2)[\rho_h^2(W-1)-W] + [1-\rho_h^4(W-1)+W]\ln R_f\}/Z, \tag{A10}$$

$$C_h = V\frac{(\rho_h^2-1)^2}{R_f^2\rho_h^2 Z}, \tag{A11}$$

with

$$W = \eta_h/\eta_f = d_h/d_f, \tag{A12}$$

$$Z = -1+\rho_h^4(1-2W)-2W+4\rho_h^2 W + 2[-1+\rho_h^4(W-1)-W]\ln\rho_h. \tag{A13}$$

For $W\to\infty$ the equations transform into the equations of Slezkin [18].

Figures 10 and 11 show the flow patterns for a solid hole ($W\to\infty$) and a fluid hole with $W=1$. The flow in the fluid hole is better visible in a flow pattern with a fixed hole in a moving film holder (Fig. 12).

Integration of the forces on the hole gives the drag on the hole:

$$F = -4\pi D_f \eta d_f = \frac{4\pi\eta d_f V}{\ln\rho_h + \dfrac{1+2W-4W\rho_h^2-(1-2W)\rho_h^4}{2[1+W+(1-W)\rho_h^4]}}. \tag{A14}$$

The second part of this equation is obtained with $D_f$ from Eq. (A9). For $W\to\infty$ (solid hole) the drag becomes

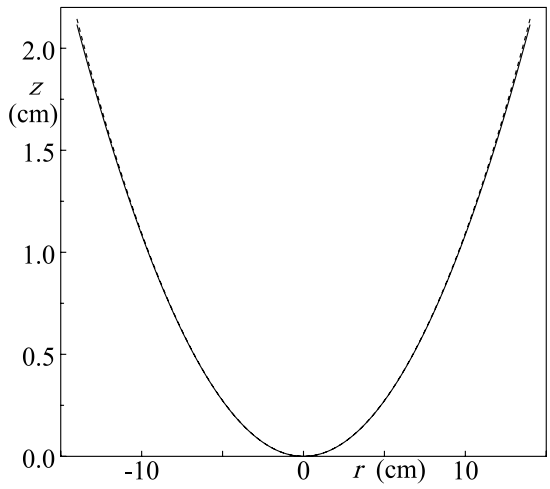


FIG. 14. Bending of a film ($A=0.04$ cm$^{-1}$) with a film radius which is approximately half of the maximum accessible value. The dashed line shows the parabolic approximation (B5). Both curves are shifted with their minima to the same value 0.

$$F_{solid} = \frac{4\pi\eta d_f V}{\ln\rho_h + (1-\rho_h^2)/(1+\rho_h^2)} \tag{A15}$$

and for $W=1$ (fluid hole)

$$F_{fluid} = \frac{4\pi\eta d_f V}{\ln\rho_h + [(\rho_h^2-2)^2-1]/4}. \tag{A16}$$

The drags on the solid and fluid hole show different dependences on the hole radius. The ratio $F_R$ is obtained as

$$F_R = \frac{F_{fluid}}{F_{solid}} = \frac{\ln\rho_h + (1-\rho_h^2)/(1+\rho_h^2)}{\ln\rho_h + [(\rho_h^2-2)^2-1]/4} \tag{A17}$$

and is shown in Fig. 13. Because $F_R$ depends on the hole radius, the determination of $\eta$ with Eq. (3) for different hole radii using $W\to\infty$ and the correct value, respectively, should allow us to differentiate between the solid and fluid hole.

## APPENDIX B: BENDING OF A FILM UNDER THE INFLUENCE OF GRAVITY

In this appendix the bending of a horizontal circular smectic film with constant thickness $d$ and density $\rho_d$ under the influence of gravity is calculated. The energy of the system consists of the potential energy of the mass and the surface energy of the film:

$$E = 2\pi\rho_d g d\int_0^{R_f} r\sqrt{1+z'^2}z\,dr + 4\pi\sigma\int_0^{R_f} r\sqrt{1+z'^2}\,dr. \tag{B1}$$

$\sigma$ is the surface tension. Some manipulations give

$$\frac{E}{4\pi\sigma} = \int_0^{R_f} r(1+Az)\sqrt{1+z'^2}\,dr, \quad A = \frac{\rho_d g d}{2\sigma}. \tag{B2}$$

The Euler-Lagrange equation of this variational problem is

$$z'' = (1 + z'^2)\left(-\frac{z'}{r} + \frac{A}{1 + Az}\right). \tag{B3}$$

The transformation $u = Ar, v = Az$ leads to

$$v'' = (1 + v'^2)\left(-\frac{v'}{u} + \frac{1}{1 + v}\right). \tag{B4}$$

We could not find an analytical solution of this equation. Numerical experiments showed that a solution is only possible for $R_f < 1.09/A$. Figure 14 shows a numerical solution of Eq. (B3) for $A = 0.04\ \mathrm{cm}^{-1}$ [$d = 25\ \mu\mathrm{m}$, density $\rho_d = 1\ \mathrm{g/cm}^3$, and surface tension $\sigma = 30\ \mathrm{mN/m}$ (8CB [7])].

For $R_f \ll 1.09/A$ the parabola

$$z = a(r^2 - R_f^2) \quad \text{with} \quad a = \frac{1 - \sqrt{1 - A^2 R_f^2}}{2AR_f^2} \tag{B5}$$

is a good approximation for the solution of the differential equation. For even smaller $R_f$ values the approximation

$$a = A/4 \tag{B6}$$

can be used.


[1] V. V. Belyaev, Russ. Chem. Rev. **58**, 917 (1989).
[2] H. Kneppe and F. Schneider, in *Handbook of Liquid Crystals*, edited by D. Demus, J. Goodby, G. W. Gray, H. -W. Spiess, and V. Vill (Wiley-VCH, Weinheim, Germany 1998), Vol. 2A, Chap. 2.5, p. 142.
[3] J. K. Moscicki, EMIS Datarev. Ser. **25**, 387 (2000).
[4] F. M. Leslie, I. W. Stewart, and M. Nakagawa, Mol. Cryst. Liq. Cryst. **198**, 443 (1991).
[5] J.-C. Géminard, R. Hołyst, and P. Oswald, Phys. Rev. Lett. **78**, 1924 (1997).
[6] H. Dumoulin, M. Brazovskaia, and P. Pieranski, Europhys. Lett. **35**, 505 (1996).
[7] F. Schneider, Rev. Sci. Instrum. **73**, 114 (2002).
[8] R. Jaquet and F. Schneider, Phys. Rev. E **74**, 011708 (2006).
[9] W. Helfrich, J. Chem. Phys. **51**, 4092 (1969).
[10] A. Zywocinski, F. Picano, P. Oswald, and J. C. Géminard, Phys. Rev. E **62**, 8133 (2000).
[11] H. Kneppe, F. Schneider, and N. K. Sharma, Ber. Bunsenges. Phys. Chem. **85**, 784 (1981).
[12] J. Thoen, in *Handbook of Liquid Crystals*, edited by D. Demus, J. Goodby, G. W. Gray, H. -W. Spiess, and V. Vill, (Wiley-VCH, Weinheim, Germany 1998), Vol. 1, Chap. 6.2, p. 310.
[13] M. G. Kim, S. Park, S. M. Cooper, and S. V. Letcher, Mol. Cryst. Liq. Cryst. **36**, 143 (1976).
[14] C. H. Sohl, K. Miyano, J. B. Ketterson, and G. Wong, Phys. Rev. A **22**, 1256 (1980).
[15] S. Bhattacharya and S. V. Letcher, Phys. Rev. Lett. **44**, 414 (1980).
[16] A. G. Krestov, S. V. Blokhina, and S. V. Kopytov, Russ. J. Phys. Chem. **63**, 206 (1989).
[17] J. Happel and H. Brenner, *Low Reynolds Number Hydrodynamics* (Martinus Nijhoff, Dordrecht, 1986), p. 394.
[18] N. A. Slezkin, *Dynamics of Viscous Incompressible Fluids* (Gos. Izdat. Tekh.-Teor. Lit., Moscow, 1955), p. 161.